Initial evaluation of the Indiana small animal PET scanner

Ned C. Rouze, *Member, IEEE,* Victor C. Soon, John W. Young, *Member, IEEE*, Stefan Siegel, *Member, IEEE*, and Gary D. Hutchins, *Member, IEEE*

***Abstract*–The Indiana small animal PET scanner is a new generation PET scanner with design goals of 1 microliter volumetric spatial resolution, a point source sensitivity of greater than 5 percent, and an imaging field-of-view suitable for whole body mouse imaging. The scanner design uses 12 planar detector banks each consisting of a 48 × 108 array of 20 mm long LSO crystals with an array pitch of 0.87 mm coupled to two Hamamatsu H8500 large area, 64-anode photomultiplier tubes. The detector modules are mounted on a rotatable gantry and are offset from the center of rotation to give an increased sampling density. Eight detector banks are currently installed in the scanner, and this report presents an initial performance evaluation of the scanner for this configuration. Using a 30 gauge needle (ID=0.15 mm, OD=0.30 mm) positioned near the center of the scanner, the transaxial resolution has been measured to be 1.1 mm FWHM and the axial resolution has been measured to be 1.5 mm FWHM. The sensitivity has been measured to be 4.0% of all decays. The scatter fraction is 0.26 and the peak noise equivalent countrate is 80 kcps at an activity of 0.22 mCi. Sample images demonstrate good imaging capabilities.**

I. Introduction

THIS report describes the design and initial performance evaluation of the Indiana small animal positron emission tomography (PET) scanner. The design goals for the scanner include a resolution of 1 mm FWHM in each of the three orthogonal directions throughout a volume suitable for whole body mouse imaging, roughly 40 mm diameter and 80 mm long. Simultaneously, the sensitivity should be 5% or greater of all decays for a point source located at the center of the scanner. A conceptual design for the scanner, including numerical simulations suggesting that it would be possible to achieve the desired performance goals, has previously been reported [1].

The scanner design uses plane detector banks mounted on a rotatable gantry. Plane detector banks allow parallax caused by oblique lines of response (LORs) to be reduced by observing coincidence events between opposing detector banks. Then individual crystals in the detectors can be lengthened to increase sensitivity and made thinner to enhance resolution. The use of high aspect ratio crystals was also guided in part by our preliminary simulations which indicated that, with plane detectors, increased crystal length does not cause significant degradation in the resolution. Rotating the detector banks allows all portions of the sinogram to be measured to obtain a complete set of measurements. Gantry rotation also allows the position of LORs to be adjusted relative to the center of rotation, thereby giving interspersed lines of response and increased sampling density.

Twelve detector banks are used in the complete scanner. Currently, 8 banks are installed, and all of the characterization measurements and images included in this report were obtained in this configuration.

II. Scanner Design

A. Detector Banks

The detector banks in the scanner take advantage of two components that have recently become available. First, the scintillation crystals consist of LSO crystal arrays manufactured by Concorde Microsystems, Inc. Fig 1(a) shows a prototype 14 × 14 array. The array consists of 20 mm long crystals with an array pitch of 0.87 mm joined with a dielectric reflector material between the crystals. The thickness of reflector and adhesive is approximately 0.07 mm so that the dead space introduced by the reflector reduces the active area of the array to 84% of the physical area. Second, fluorescence from the crystals is detected by Hamamatsu H8500 PMTs, one of which is pictured in Fig. 1(b). These PMTs are 52 mm square and have an active area of 49 mm square. Signal readout is performed using an 8 × 8 grid of anodes with a spacing of 6.08 mm. As shown in Fig. 1(c), a complete detector bank uses a 48 × 108 crystal array, with fluorescence detected using two H8500 PMTs. Fig. 1(d) shows a packaged detector module. Mu-metal shielding is used to reduce stray magnetic fields, and the detector package includes mounting flanges to position the module on the gantry. Bleeder resistors are used to compensate for the variable gain of individual anodes.

To increase the countrate capacity, the 48 × 108 crystal array is divided into 12 subarrays, and detector electronics are used to process signals from each subarray independently. The scanner uses the "pico-3D" detector electronics from CPS Innovations, Inc. Each channel accepts inputs from an

Manuscript received November 11, 2005. This work was supported by the state of Indiana 21st Century Research and Technology Fund "Indiana Center of Excellence in Biomedical Imaging" and by the Indiana Genomics Initiative. The Indiana Genomics Initiative (INGEN) is supported in part by Lilly Endowment, Inc.

N. C. Rouze, V. C. Soon, and G. D. Hutchins are with the Department of Radiology, Division of Imaging Science, Indiana University School of Medicine, Indianapolis, IN 46202 USA (telephone 317-274-2067, email nrouze@iupui.edu, vsoon@iupui.edu, and gdhutchi@iupui.edu).

J. W. Young is with CPS Innovations, Inc., Knoxville, TN 37932 USA (email John.Young@cpspet.com).

S. Siegel is with Concorde Microsystems, Inc., Knoxville, TN 37932 USA (email ssiegel@cms-asic.com)

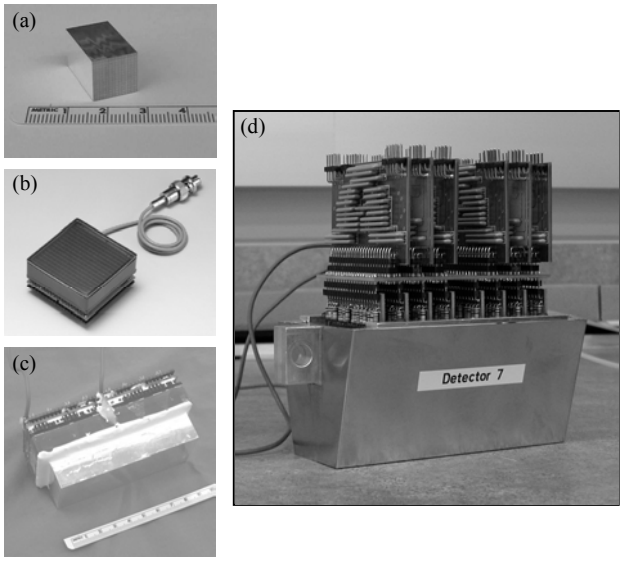

Fig. 1. (a) Sample 14 × 14 crystal array consisting of 20 mm long LSO crystals with an array pitch of 0.87 mm. (b) Hamamatsu H8500 large-area multianode PMT. (c) Each detector bank uses two H8500 PMTs to detect light from a 48 × 108 crystal array. (d) Packaged detector showing the mounting flange, mu-metal shield, and bleeder and positioning resistors.

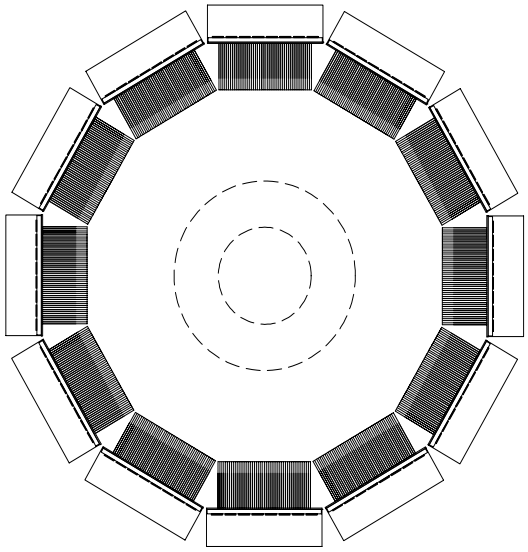

Fig. 3. Layout of the complete scanner. Twelve detectors are arranged in a 160 mm diameter ring. For coincidence events between opposing detector banks, the FOV is 41.7 mm (inner dashed circle). For coincidence events between each detector bank and the opposing and adjacent (tilted) banks, the FOV is 81.7 mm (outer dashed circle). Eight detectors are currently installed.

ordinary 4-PMT block detector and determines the time, the X and Y position coordinates within the block, and the energy of the fluorescence signal. Resistor networks are used to combine the 128 anode signals in the detectors to simulate the output of ordinary 4-PMT detector blocks. For each subarray, anode signals from a set of 4 × 5 or 5 × 5 anodes extending slightly beyond the desired crystal range are used. Each anode within this set is connected through a resistor to each of the four electronics inputs with the individual resistance values chosen according to the X and Y positions of the anode within the set, and with the constraint that the parallel combination of resistances is 1670 Ω. Because the anode sets extend beyond the subarray crystal ranges, the anodes sets overlap and individual anodes can contribute to one, two, or four channels. This variation is taken into account when selecting values of the bleeder resistors.

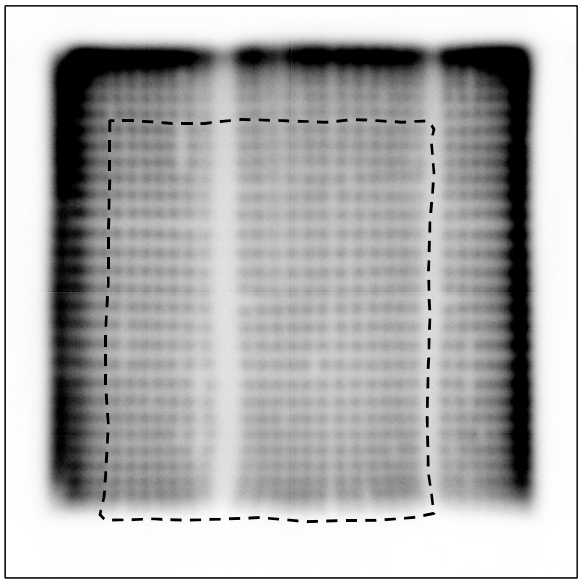

Fig 2. Position profile for one subarray showing the ability to identify all crystals. For this case, the dashed curve encloses a 19 × 24 region of crystals.

A sample position profile from one crystal subarray is shown in Fig. 2. In this particular case, it was desired to identify a 19 × 24 subarray of crystals as indicated by the dashed line on the profile. Other crystals in the 48 × 108 array surround this subarray on three sides causing the bright band in the profile. However, within the desired range, all crystals are easily identified. Similar profiles show easy identification of all crystals in the entire 48 × 108 array, even across the gap between the two PMTs.

B. Rotatable Gantry

As shown in Fig. 3, the detector banks are mounted on a rotatable gantry in a 160 mm diameter ring. The final scanner configuration will use 12 detector banks. Currently, only 8 detectors are installed, and all of the performance evaluation measurements and images presented in this report were acquired in this configuration. When only coincidence events between opposing detector banks are used, the field of view (FOV) is 41 mm. Typically, events between each detector and the opposing 3 detectors are recorded giving a FOV of 81 mm.

Coincidence events are identified using a coincidence board from CPS innovations, Inc. with an 8 ns coincidence window. Data are collected during continuous gantry rotation with a typical rotation rate of 2 rpm. Events are transferred from the gantry using a capacitive coupled slipring from CPS Innovations, Inc. and are saved to disk in list mode format. The gantry position is determined using an angular position encoder attached to the drive motor, and tag events are inserted into the event stream every 20 ms. A pin on the parallel port of the acquisition computer is toggled synchronously with the tag insertion to allow external devices

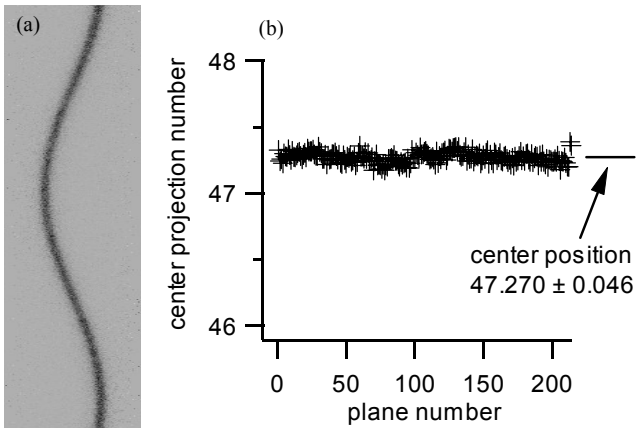

Fig. 4. (a) Sinogram from one plane using an axial source. (b) Center of rotation position as determined using all 8 detector banks currently installed in the scanner.

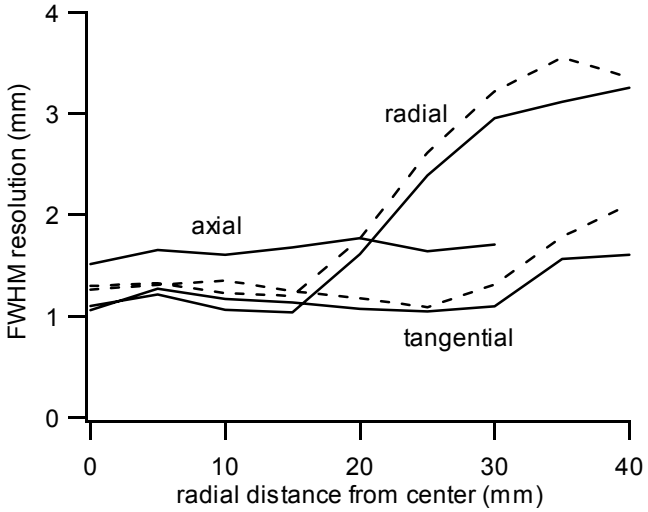

Fig.5. FWHM resolution in the radial, tangential, and axial directions as a function of radial distance from the center of the scanner FOV. Two results are given for the radial and tangential directions - the solid curves show the results obtained using interspersed LORs, and the dashed curves show the results obtained without the use of interspersed LORs.

such as EKG monitors to be synchronized with the event stream.

Shim washers are used to adjust the transaxial position of the detectors relative to the center of rotation. With 48 transaxial crystals, there are 95 direct and cross LORs, numbered 0-94, in each plane between opposing detector banks. The shim washers are chosen to position the detector banks so that the center of rotation is located at LOR 47.25. Thus, after a gantry rotation of 180 degrees, the new LORs will be interspersed with the original set of LORs, giving increased sampling density. This procedure has been shown [2] to increase the resolution by roughly 20% compared to the case without interspersed LORs. A similar increase is expected for this scanner [1], and the resolution measurements presented in Sec. 3 indicate that the increase is realized.

To determine the position of the center of rotation, we use a line source oriented axially in the scanner and displaced slightly from the center. Fig. 4(a) shows one plane of the sinogram $g(s,\phi)$ obtained with this source which shows the expected sinusoidal shape. This sinogram was fit with a two dimensional function of the form

$$g(s,\phi) = A\exp(-(s - s_0(\phi))^2 / \sigma^2)$$

where

$$s_0(\phi) = B\sin(\phi + \phi_0) + s_{cent}$$

Thus, the projection number s_{cent} corresponding to the center of rotation can be determined. Using the default shim washers, this value was determined for each pair of opposing detectors, and the shim washers were adjusted so that s_{cent} would be as close to 47.25 as possible. Fig. 4(b) shows the resulting values of s_{cent} measured with all of the detector pairs for each of the 215 scanner planes. The average value is 47.270 ± 0.046 projection numbers. Using the projection spacing of one half the crystal pitch, this standard deviation corresponds to a distance of 20 μm.

After acquisition, data are sorted into sinograms using 512 angular coordinates in 360 degrees. Deadtime and randoms corrections are software controllable, however these corrections are applied in the default case. The range of oblique planes is limited using a plane window of 48, and sinograms are sorted using a span of 5 [3] to reduce parallax and give better axial resolution. Fourier rebinning [3] is used to combine oblique sinogram data into axial planes. Filtered backprojection (FBP) with ramp or Hanning filters is used for all image reconstruction.

III. Performance Evaluation

A. Resolution

The scanner resolution was measured using F-18 in a 30 gauge needle (ID=0.15 mm, OD=0.30 mm) mounted on a translation stage. First, the needle was oriented parallel to the axis of the scanner near the center, and data were collected as a function of the needle position as it was moved toward the edge of the FOV. These data sets were reconstructed using FBP with a ramp filter to give the radial and tangential components of the resolution. No correction was made for the size of the source. This process was repeated with the needle oriented transaxially to determine the axial resolution.

Fig. 5 shows the FWHM resolution as a function of the source position. Two results are shown for the radial and tangential measurements, the solid curves give the resolution determined when interspersed lines of response were included in the sorted data, and the dashed lines indicate the results when only noninterspersed LORs were used. At the center of the FOV, the resolution is approximately 1.1 mm FWHM when interspersed lines of response are used. This value is approximately 20% better than the case without using interspersed lines of response, in rough agreement with previous observations [2]. As expected, when moving away from the center of the FOV, the tangential resolution is approximately independent of position, while the radial resolution increases due the greater influence of parallax in the measurements. The axial resolution is approximately 1.5 mm

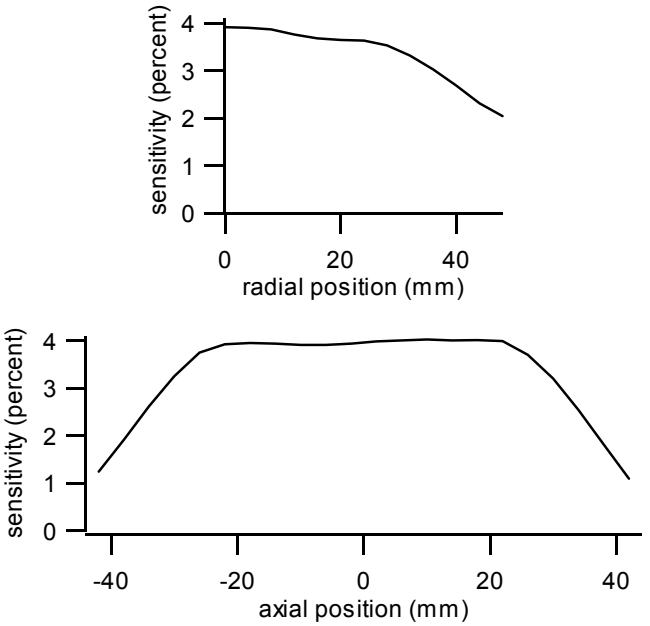

Fig. 6. Measured sensitivity, reported as a percentage of all decays, as a function of the radial and axial source position relative to the center of the scanner.

FWHM and is approximately independent of position. The combination of radial, tangential, and axial resolution give a volume resolution of less than 1.8 μl at the center of the FOV.

B. Sensitivity

The sensitivity was measured using a droplet of FDG placed in a 1.5 mm diameter hole at the center of a 6 mm diameter acrylic rod. The source activity, measured calibrated well counter, was chosen to be sufficiently low (roughly 10 μCi) so that deadtime and random coincidences were less than 1%. The source was positioned at the center of the FOV on a translation stage and 1 min. data sets were collected at source positions along the axis of the scanner and at radial displacements from the center of the scanner. Each data set was sorted into sinograms using the same windows and randoms subtraction used for ordinary image data, and the total number of events determined. These values were compared to the number of decays, corrected for the time difference between source calibration and acquisition, and for the 97% branching ratio between decays and positron emission with F-18.

Fig. 6 shows the measured sensitivity as a function as axial and radial position in the scanner. We observe that the peak sensitivity is approximately 4% of all decays. The sensitivity exhibits only a weak dependence as a function of radial position, and is approximately constant along the scanner axis due to the axial window that restricts the range of tilt angles for oblique LORs.

C. Countrate performance

The countrate performance of the scanner was characterized using a decaying source to measure the noise equivalent countrate (NEC) [4]. Initially, 10 mCi of C-11 labelled acetate was placed in a 45 mm diameter, 37 mm long cylindrical phantom centered in the scanner, and data sets were collected

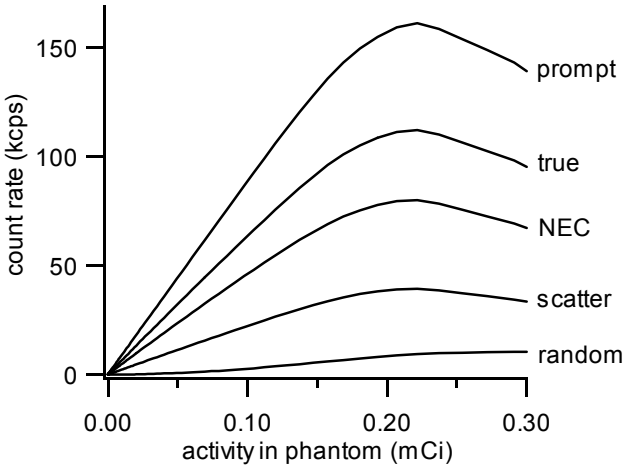

Fig. 7. Prompt, true, NEC, scatter, and random countrates as a function of activity. The peak NEC is 80 kcps at an activity of 0.22 mCi.

periodically over a period greater than 12 half lives. The prompt P and random R countrates were measured as a function of activity, and the NEC was calculated according to the relation

$$NEC = \frac{T^2}{T + S + 2kR}$$

where k is the fraction of the FOV occupied by the phantom, k=0.55, T is the true countrate,

$$T = (P - R) \times (1 - SF),$$

S is the scatter countrate

$$S = (P - R) \times SF,$$

and SF is the scatter fraction. The scatter fraction was measured using a homemade phantom similar to the NEMA phantom [5] used to measure the scatter fraction in clinical PET scanners. The phantom consisted of a 38 mm diameter, 150 mm long polyethylene cylinder with a plastic tube (2.0 mm ID, 3.2 mm OD) inserted in a hole parallel to the axis and offset from the axis by 10 mm. Roughly 10 μCi of FDG was inserted in the tube, and the phantom was scanned for 10 minutes. The scatter fraction was calculated in the same manner as for the NEMA standard - sinogram profiles were shifted to align the peak locations and then summed over angles, a Gaussian function was fit to the tails of the summed profile, and the scatter fraction calculated as the ratio of the signal in the tails compared to the total signal. The scatter fraction was determined to be 0.26.

Fig. 7 shows the prompt, true, random, scatter, and NEC countrates as a function of activity in the phantom. In particular, we observe that the NEC reaches a peak of more than 80,000 cps at an activity of 0.22 mCi.

D. Sample Images

Samples images acquired with the scanner are shown in Figs. 8 - 10. Fig. 8 shows images acquired using the hot spot and cold spot inserts in the Data Spectrum Micro-Deluxe phantom. These inserts consist of six sets of holes (hot spots) or rods (cold spots) with diameters of 4.8, 4.0, 3.2, 2.4, 2.6, and 1.2 mm. For each set, the spacing of the holes or rods is equal to twice their diameter. The images were acquired using

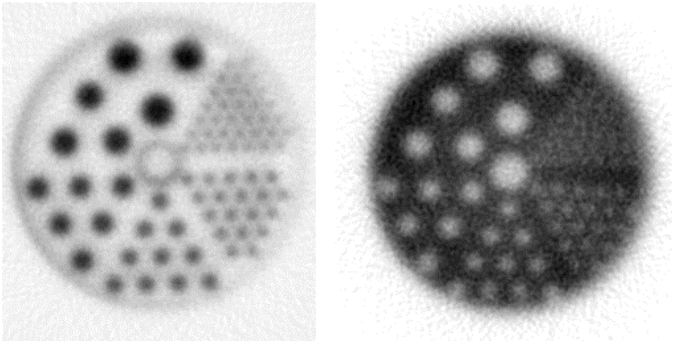

Fig. 8. Images obtained using the hot spot (left) and cold spot (right) inserts in the Data Spectrum Micro-Deluxe phantom. The diameters of the holes and rods in the inserts are (counterclockwise from top) 4.8, 4.0, 3.2, 2.4, 1.6, and 1.2 mm. The spacing of holes and rods is twice their diameter.

an initial activity of roughly 0.3 mCi FDG and imaging the phantom for 3 hours. Images were reconstructed using FBP with a ramp filter, and 20 image planes were summed to reduce noise. We observe that the hot spots in each of the sections in Fig. 8(a) can easily be resolved. The 1.6 mm cold spots in Fig. 8(b) can be resolved, but not the 1.2 mm spots.

Fig. 9 shows three maximum intensity projection (MIP) images collected in a fluoride scan of a 245 g rat. The data were collected under normal imaging conditions using a 1 mCi injection, a 45 min. uptake period, and a 30 min. acquisition. Images were reconstructed using FBP with a Hanning filter with cutoff at 70% of the Nyquist frequency.

Fig. 10 shows three MIP images of a 19.5 g mouse. This is an example of a transgenic model that spontaneously develops neurofibromas. A tumor is clearly seen under the spine near the center of the back. These images were collected under normal conditions using an injection of 0.29 mCi, 45 min. uptake, 30 min. data acquisition, one bed position, and image reconstruction using FBP with a 70% cutoff Hanning filter.

IV. Summary

In summary, the performance of the Indiana small animal PET scanner has come close to the design goals. The radial and tangential resolution of 1.1 mm FWHM at the center of the FOV are very close to the design goals. The axial resolution of 1.5 mm FWHM and volume resolution of 1.8 ul are not quite as good as the design goals, but are still quite

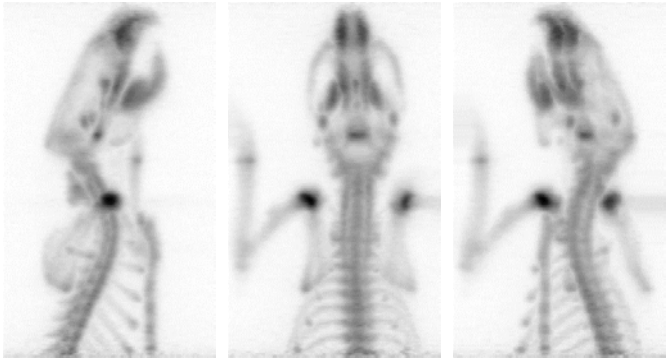

Fig. 9. Three MIP images at different orientations obtained in a fluoride bone scan of a 245 g rat.

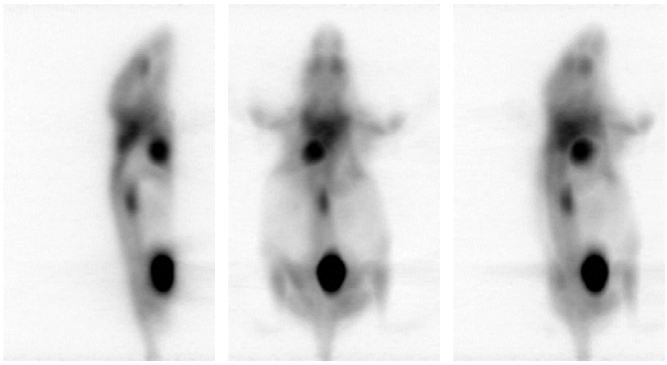

Fig. 10. Three MIP images of a 19.5 g mouse. This mouse is an example of a transgenic model that spontaneously develops neurofibromas, for example, the tumor just under the spine at the center of the back.

reasonable for a small animal PET scanner. When the final four detectors are installed, the sensitivity is expected to increase to approximately 6%, exceeding the design goals. Furthermore, the sensitivity is greatly limited because of the plane window restriction of 48 crystals. If all oblique planes with crystal differences up to the maximum of 108 crystals were included, the sensitivity would more than double for a point source located at the center of the FOV. We expect that this restriction can be removed when the system matrix is measured and iterative reconstruction methods are used to account for parallax in LORs with large oblique angles. The counting capability is good and will improve with the additional detectors. Finally, we are quite pleased with the imaging capabilities.

Acknowledgments

This project would not have been possible without important contributions from many individuals. In particular, we thank Robert Nutt from Concorde Microsystems, Mark Musrock, Bill Jones, Johnny Reed, Chad Seaver, Matthias Schmand, Ken Baker, and Ron Nutt from CPS Innovations, Inc., Keith Vaigneur and Dave Willis from Agile Engineering, Inc., and Michael Miller and Tim Receuver from Indiana University School of Medicine.

References

[1] N. C. Rouze, M. Schmand, S. Siegel, and G. D. Hutchins, "Design of a Small Animal PET Imaging System with 1 Microliter Volume Resolution," *IEEE Trans. Nuc. Sci*., vol. 51, 757-763, 2004.

[2] N. C. Rouze and G. D. Hutchins, "Design and Characterization of IndyPET-II: A High-Resolution, High-Sensitivity Dedicated Research Scanner, *IEEE Trans. Nuc. Sci*., vol. 50:1491-1497, 2003.

[3] M. Defrise, P. E. Kinahan, D. W. Townsend, C. Michel, M. Sibomana, and D. F. Newport, "Exact and Approximate Rebinning Algorithms for 3-D PET Data," *IEEE Trans. Med. Img.,* vol. 16, pp. 145-158, 1997.

[4] S. C. Strother, M. E. Casey, and E. J. Hoffman, "Measuring PET scanner sensitivity: relating countares to image signal-to-noise-ratios using noise equivalent counts, *IEEE Trans. Nuc. Sci.*, vol. 37, 783-788, 1990.

[5] NEMA Standards Publication NU 2-2001, Performance Measurements of Positron Emission Tomographs," National Electrical Manufacturers Association, Rosslyn VA 22209.